

Semi-linear gravitational lens inversion

S. J. Warren and S. Dye

Astrophysics Group, Blackett Laboratory, Imperial College London, Prince Consort Road, London, SW7 2BW, UK

ABSTRACT

We describe a new method for analyzing gravitational lens images, for the case where the source light distribution is pixelized. The method is suitable for high resolution, high S/N data of a multiply-imaged extended source. For a given mass distribution, we show that the step of inverting the image to obtain the deconvolved pixelized source light distribution, and the uncertainties, is a linear one. This means that the only parameters of the non-linear problem are those required to model the mass distribution. This greatly simplifies the search for a $\text{min.} -\chi^2$ fit to the data and speeds up the inversion. The method is extended in a straightforward way to include linear regularization. We apply the method to simulated Einstein ring images and demonstrate the effectiveness of the inversion for both the unregularized and regularized cases.

Subject headings: gravitational lensing

1. Introduction

This paper is concerned with the problem of inversion of a gravitationally-lensed image of an extended source, i.e. a galaxy rather than a star or quasar. This problem is interesting because lensed images of extended sources provide more information than images of point sources, and so potentially are more useful for determining the mass profiles in galaxies and clusters of galaxies. Also, because of the magnification, one can measure structure in the light profile of the source at enhanced resolution. In this paper we show how this problem can be separated in a natural way into linear and non-linear dimensions, and how this provides a number of advantages.

In this introduction we review solutions to the inversion problem and introduce some of the terminology used in the remainder of the paper. In all the solutions described here the mass in the lens is parameterized. Nevertheless the analysis applies equally to a pixelized mass distribution.

When presented with the lensed image of an extended source, the unknowns to solve for are the source light profile and the lens mass profile, and the uncertainties in these quantities. One approach to this problem, suggested by Kayser and Schramm (1988), uses the fact that regions of the source that are multiply-imaged have the same surface-brightness. For a trial mass distribution, the method traces image pixels to the source plane where the counts in different image pixels mapping to the same source pixel are compared. The solution for the mass is obtained by minimizing the dispersion in the image pixel counts for such multiply-imaged source pixels. Kochanek et al. (1989) successfully applied this approach to the inversion of the radio Einstein ring MG1131+0456. The algorithm was refined by Wallington, Kochanek, and Koo (1995) who applied it to the triply-imaged giant arc in the galaxy cluster Cl 0024+1654.

The main shortcoming of this approach is that it does not deal with the image point-spread-function (psf). If psf smearing of the image (either instrumental or atmospheric) is significant, the light profile of the source is not correctly recovered by backward tracing the image, even if the mass distribution is exactly known. To deal with the psf, a forward approach is needed i.e. one chooses a model for the source light profile (parameterized or pixelized), and a model for the mass (parameterized or pixelized), forms the image, convolves it with the psf, and compares it to the actual image, adjusting the source and lens models to minimize a merit function e.g. χ^2 .

An argument for choosing to parameterize rather than pixelize the source light profile is that it forces the solution to be smooth. Nevertheless, the source light profile may be complex. This is true, for example, in the cases of MG1131+0456 and Cl0024+1654, cited above. A large number of parameters might be required to provide a satisfactory description. Without clues to the character of the source it is extremely difficult to select the best parameterization i.e. the one which provides a satisfactory fit with the smallest number of parameters. In the most extreme example Tyson, Kochanski, & dell'Antonio (1998) used 232 parameters to model the source light distribution of the galaxy lensed by the cluster Cl0024+1654.

If the source light profile is complex it is natural to consider pixelizing the source, i.e. the counts in each pixel is a free parameter. This removes the difficulty in finding a good parameterization for the source, and thereby avoids any bias in the fitted mass profile resulting from a poor choice. On the other hand, due to the deconvolution, and because the pixels are independent, the solution can be noisy. It is possible to achieve a smooth pixelized solution by adding a suitable ‘regularizing’ term to the merit function. This term, if minimized on its own, would produce a smooth source light profile. By adding this term to χ^2 the final solution involves a balance between obtaining the best fit to the image (minimizing

χ^2), and obtaining a smooth source solution (minimizing the regularizing term). Wallington, Kochanek, and Narayan (1996) apply this approach to the case of the radio Einstein ring MG 1654+134. They use a maximum entropy approach i.e. the regularizing term to be minimized is the negative of the entropy, the negentropy. Labeling the counts in source pixel i by s_i , the source plane negentropy is $\sum_i s_i \ln(s_i)$, and the merit function they minimize is

$$G = \chi_{im}^2 + \lambda \sum_i s_i \ln(s_i) \quad (1)$$

(here we have followed the notation in Press et al., 2001, §18.7). The purpose of the multiplier λ is to give more or less weight to the negentropy term.

The inversion proceeds as follows: For a fixed value of λ , the solution is determined by searching through the multi-parameter space for the minimum of the merit function. The number of dimensions of the parameter space to search is the sum of the number of source pixels and the number of parameters used for the mass. This search is most efficiently achieved with a pair of nested cycles. The inner (source) cycle searches for the best source light profile for a fixed mass profile. The outer (mass) cycle adjusts the mass profile. Outside this cycle is a third (λ) cycle where the multiplier is adjusted. Because the negentropy term acts to smooth the source, as λ increases, the χ_{im}^2 term also increases, i.e. the fit becomes worse. The principle for reaching the final solution (e.g. Press et al., 2001, §18.4) is to start with λ large, then progressively reduce the weight of the regularizing term until the χ_{im}^2 becomes satisfactory. In other words the solution has the smoothest source that provides a satisfactory fit to the image. ‘Satisfactory’ is usually interpreted as reaching the criterion for the χ^2 for the image $\chi_{im}^2 = \min(\chi_{im}^2) + \sigma(\chi_{im}^2)$. With three nested cycles, the λ , mass, and source cycles, the routine can be slow.

In this paper we describe a new technique which we suggest simplifies and clarifies the problem in a number of ways. In purely formal terms, the method is very similar to the maximum entropy method of Wallington et al.: Algebraically, we simply replace the negentropy term in the merit function (1) with a linear regularization term. However, the insight we bring is to show that for a fixed mass distribution, the minimization of the merit function is now a linear problem i.e. can be solved by matrix inversion. In other words the source cycle – the innermost of the three minimization cycles – is eliminated. This has major benefits. In the first place the inversion is much quicker, thereby allowing a more thorough search for the best fit mass model. At the same time, the uncertainty of identifying the true minimum has been removed. The method also greatly simplifies calculation of the uncertainties, as we show below. More generally, the formalism clarifies the essence of the problem: The source parameters are linear dimensions and the mass parameters are non-linear dimensions. For this reason we call the method ‘semi-linear’.

At this point it is worth noting that, because of magnification and multiple imaging, the number of constraints to the solution can be much greater than the number of parameters to solve for. In this respect the lens inversion problem differs from many inversion problems encountered in astronomy (for example image deconvolution). We find, as a consequence, that in many circumstances the regularization term can be removed altogether. So the λ cycle is also eliminated. The merit function is then just χ_{im}^2 , and this is our starting point for the presentation of the theory. For a fixed mass profile, the pixelized source light distribution that produces the min.- χ_{im}^2 fit is obtained by linear inversion. The mass profile is then adjusted to find the minimum of these min.- χ_{im}^2 fits. The advantage, besides speed (only the mass cycle remains), is that the solution is unbiased, since there is no smoothing of the source.

The outline of the remainder of the paper is as follows. In §2 we explain the basic theory, demonstrating that for a fixed mass profile, the problem of obtaining the source light profile by χ^2 minimization in the image plane is a linear one, and obtaining the covariance matrix for the counts in the source pixels. We then extend the basic theory to include a linear regularization term. In §3 we apply the method to a realistic problem, assessing the performance for different psf widths, and different source pixel sizes, with and without linear regularization. In §4 we provide a summary of the main points, together with recommendations for applying the method.

2. Theory

In this section we present the theory of semi-linear inversion, firstly without regularization (§2.1), and then with regularization (§2.2). In each sub-section we begin with the case where the mass is fixed, and then treat the general case, minimizing also on the mass parameters.

2.1. Semi-linear inversion without regularization

2.1.1. Fixed mass: Eliminating the source cycle

Without any regularizing term, the merit function is simply $G = \chi_{im}^2$. The basic problem is to find the counts in the source pixels that, for a given mass distribution, minimize the merit function G , i.e. give the best fit to the observed image. Pixels in the source plane are labeled $i = 1, I$. There is no restriction on how the source plane is tessellated. In principle, the pixels could change in both size and shape across the source region, which itself could be

of any shape. Pixels in the image plane are labeled $j = 1, J$. It is assumed in the following that the image pixels include counts from the image of the lensed source only i.e. the images of any lensing galaxies, and the mean sky count, have been subtracted. Also we suppose that the data in each image pixel are independent i.e. are characterized by the counts d_j , and dispersion σ_j , with no covariance between pixels (appropriate for CCD data).

The inversion proceeds as follows: Choose the mass model parameters, then, for each source pixel i , in turn, form the image for unit counts (surface brightness) by appropriate ray tracing and convolution with the known point spread function i.e. compute the counts in the i th image $f_{ij}, j = 1, J$. The problem now is to combine these I images with scalings $s_i, i = 1, I$, to minimize G . These scalings are the deconvolved intrinsic source surface-brightness distribution.

The problem is of a standard type. The merit function is written

$$G = \chi_{im}^2 = \sum_{j=1}^J \left[\frac{\sum_{i=1}^I s_i f_{ij} - d_j}{\sigma_j} \right]^2. \quad (2)$$

Minimizing with respect to each of the source terms we have a set of I simultaneous equations of the form

$$\frac{1}{2} \frac{\partial G}{\partial s_i} = 0 = \sum_{j=1}^J \left[\frac{f_{ij} \sum_{k=1}^I s_k f_{kj} - f_{ij} d_j}{\sigma_j^2} \right] \quad (3)$$

where the reason for the factor $\frac{1}{2}$ will soon become clear. These equations may be written in matrix form

$$\mathbf{F}\mathbf{S} = \mathbf{D}. \quad (4)$$

Here \mathbf{S} is a column matrix of length I containing the elements s_i , to be solved for. \mathbf{F} is a symmetric $I \times I$ matrix, with elements $\mathbf{F}_{ik} = \sum_{j=1}^J f_{ij} f_{kj} / \sigma_j^2$. Finally \mathbf{D} is a column matrix of length I containing the elements $\mathbf{D}_i = \sum_{j=1}^J f_{ij} d_j / \sigma_j^2$.

The solution for the counts in the source pixels is then simply obtained by matrix inversion

$$\mathbf{S} = \mathbf{F}^{-1} \mathbf{D} \quad (5)$$

thus eliminating the source cycle.

The solution for the errors has a particularly simple form. We seek the covariance matrix for the source pixels. Noting that

$$\mathbf{F}_{ik} = \frac{1}{2} \frac{\partial^2 G}{\partial s_i \partial s_k}, \quad (6)$$

we see that the matrix \mathbf{F} is one half times the Hessian matrix of χ_{im}^2 , which is to say that \mathbf{F} is the *curvature matrix* of the problem (Press et al., 2001, §§15.4, 15.5) – this was the reason for using the factor $\frac{1}{2}$ in equation (3). We now show that the matrix $\mathbf{C} = \mathbf{F}^{-1}$ is the required covariance matrix of \mathbf{S} .

For independent image pixels, the covariance between source pixels i and k is given by

$$\sigma_{ik}^2 = \sum_{j=1}^J \sigma_j^2 \frac{\partial s_i}{\partial d_j} \frac{\partial s_k}{\partial d_j}. \quad (7)$$

Using equation (5) this becomes

$$\sigma_{ik}^2 = \sum_{j=1}^J \sigma_j^2 \sum_{l=1}^I \mathbf{C}_{il} \frac{f_{lj}}{\sigma_j^2} \sum_{m=1}^I \mathbf{C}_{km} \frac{f_{mj}}{\sigma_j^2}. \quad (8)$$

Multiplying this out gives

$$\sigma_{ik}^2 = \mathbf{C}_{ik} \quad (9)$$

as required.

We see that for the case of fixed mass, the covariance matrix for the source pixel counts is computed in the inversion step, without the need for further calculation. We shall refer to this $I \times I$ matrix as the *source covariance matrix* hereafter. Even though it is not the complete solution for the source pixel errors (because the mass parameters have been fixed), the source covariance matrix is extremely useful, for example, in exploring different mass models and pixelizations (§3).

It is worth noting that the semi-linear inversion solution, either with or without regularization, differs in character from the maximum entropy solution. With the semi-linear method the counts in any source pixel are unbounded, so the best-fit value could be negative, since some image pixels contain negative counts (i.e. are below mean sky). With the maximum entropy method all source counts must be positive. The semi-linear method provides the best estimate of the counts in a source pixel, and the solution is satisfactory provided the result is consistent with being positive. If the counts in any source pixel are significantly negative (e.g. $< -4\sigma$) this would indicate a bad mass model. This possibility of testing the suitability of the mass model with a source-plane statistic can be viewed as an extra positive feature of the semi-linear method.

2.1.2. Mass cycle

The full solution proceeds by searching through the mass-distribution parameter space, at each point minimizing χ_{im}^2 by linear inversion, to find the smallest of these min.– χ_{im}^2 values, the global minimum. Because the number of dimensions of the parameter space for the non-linear search has been greatly reduced, it is now a much simpler problem to locate the true minimum securely.

The solution for the errors is more complicated than above, since we have added in the non-linear mass dimensions. If there are L parameters that describe the mass, labeled m_l , we need to form the $(I+L) \times (I+L)$ (symmetric) curvature matrix of the problem. But note that the majority of the terms, the $I \times I$ terms $\frac{1}{2} \frac{\partial^2 G}{\partial s_i \partial s_k}$, have already been computed and are the elements of the matrix \mathbf{F} at the global minimum. The remaining terms, the L rows (and columns) of terms such as $\frac{1}{2} \frac{\partial^2 G}{\partial m_l \partial m_n}$, and $\frac{1}{2} \frac{\partial^2 G}{\partial m_l \partial s_i}$, can be filled in by simple measurement of the shape of the χ_{im}^2 surface about the global minimum. The covariance matrix for the mass and source parameters is the inverse of this curvature matrix. We shall refer to this $(I+L) \times (I+L)$ matrix as the *full covariance matrix* hereafter.

2.2. Semi-linear inversion with regularization

2.2.1. Fixed mass: Eliminating the source cycle

The possibility of replacing the negentropy term in equation (1) by a term (a linear regularization term) which preserves the linearity of the min.– χ^2 approach is made evident by the linearity of equation (3) with respect to the source parameters. Clearly we can form a merit function by adding to χ_{im}^2 any term G_L which is a linear combination of terms $s_i s_k$

$$G_L = \sum_{i,k} a_{ik} s_i s_k \quad (10)$$

since the partial differentials of these additional terms will also be linear. One example of a linear regularization term is $G_L = \sum_{i=1}^I s_i^2$. The choice of G_L is discussed below.

Writing the merit function generally as

$$G = \chi_{im}^2 + \lambda G_L \quad (11)$$

then, following through the same analysis as in §2.1.1, the solution for the counts in the source pixels can be written

$$\mathbf{S} = [\mathbf{F} + \lambda \mathbf{H}]^{-1} \mathbf{D}. \quad (12)$$

We call the matrix \mathbf{H} the regularization matrix. The elements of \mathbf{H} are

$$\mathbf{H}_{ik} = \frac{1}{2} \frac{\partial^2 G_L}{\partial s_i \partial s_k}. \quad (13)$$

For example, if the regularization term is $G_L = \sum_{i=1}^I s_i^2$, then we have $\mathbf{H} = \mathbf{I}$, the identity matrix.

The form of G_L should be chosen to penalize noisy solutions. The choice $G_L = \sum_{i=1}^I s_i^2$, termed “zeroth-order” regularization in the literature, is one attempt to achieve this. Other widely-used linear regularization terms include *gradient* and *curvature* forms. These three regularization forms correspond, loosely speaking, to the prejudice that the source light profile is, respectively, approximately zero, constant, or planar (see Press et al., 2001, §18.5, for a detailed account of the theory of linear regularization and its implementation). In practice, if λ is not too large, all three terms serve to smooth the source in a rather similar way, and there is little to distinguish between the solutions.

The gradient and curvature forms consider the differences between counts in neighboring pixels. Until now we have used a one-dimensional numbering scheme for the source pixels. In this case, since we need to take account of the relative spatial locations of pixels in the source plane we use coordinates x, y . The simplest gradient term is

$$G_L = \sum_{x,y} [s_{x,y} - s_{x+1,y}]^2 + \sum_{x,y} [s_{x,y} - s_{x,y+1}]^2. \quad (14)$$

Another form uses $[s_{x,y} - 0.5(s_{x+1,y} + s_{x,y+1})]^2$. In forming the sum it is necessary to translate the indices x, y to the index i , and then equation (13) is used to form the matrix \mathbf{H} . Note that zeroth-order regularization is computationally by far the simplest method, since it does not involve this step of translation of indices.

The simplest curvature form is

$$\begin{aligned} G_L = & \sum_{x,y} [s_{x,y} - 0.5(s_{x-1,y} + s_{x+1,y})]^2 \\ & + \sum_{x,y} [s_{x,y} - 0.5(s_{x,y-1} + s_{x,y+1})]^2. \end{aligned} \quad (15)$$

Another form uses $[s_{x,y} - 0.25(s_{x-1,y} + s_{x+1,y} + s_{x,y-1} + s_{x,y+1})]^2$.

The source covariance matrix for the regularized case is fortunately only slightly more difficult to compute than for the unregularized case. Writing $\mathbf{R} = [\mathbf{F} + \lambda \mathbf{H}]^{-1}$, and following the same line of reasoning as in §2.1.1, we obtain the analogous equation to equation (8)

$$\sigma_{ik}^2 = \sum_{j=1}^J \sigma_j^2 \sum_{l=1}^I \mathbf{R}_{il} \frac{f_{lj}}{\sigma_j^2} \sum_{m=1}^I \mathbf{R}_{km} \frac{f_{mj}}{\sigma_j^2}. \quad (16)$$

Multiplying out we obtain

$$\sigma_{ik}^2 = \mathbf{R}_{ik} - \lambda \sum_{l=1}^I \mathbf{R}_{il} [\mathbf{RH}]_{kl}. \quad (17)$$

2.2.2. Mass cycle

The procedure for the full solution is the same as for the unregularized case. One searches through the mass–distribution parameter space, at each point minimizing G by linear inversion, to find the smallest of these $\min.-G$ values, the global minimum. In the regularized case there is no simple solution for the full covariance matrix however. In the unregularized case, we were able to use the fact that the inverse of the full curvature matrix is the full covariance matrix. But in the regularized case this is no longer true since we are minimizing $G = \chi_{im}^2 + G_L$. Instead, an alternative approach must be used, for example, a Monte Carlo method which inverts an ensemble of realisations of the image by adding noise to the original image.

3. Simulations

In this section we apply the semi–linear inversion method to a realistic test problem. To validate the linear inversion step, we begin with the case of fixed mass. We quantify the effectiveness of the method under variations of the image S/N , psf width, and source pixel size, for both the unregularized and regularized cases. We then present an analysis of the full problem, allowing the mass parameters to vary. Finally we debate the advantages of the unregularized and regularized approaches, for different practical applications.

3.1. Test problem

To make the computations more useful we have based our investigation on a realistic simulation of a deep image of an Einstein ring gravitational lens system observed with the Advanced Camera for Surveys (ACS) aboard HST. The camera has a pixel size of $0.05''$. We have used cosmological parameters $\Omega_m = 0.3$, $\Omega_\Lambda = 0.7$. The lens is placed at $z = 0.3$ and the source lies at $z = 3.0$.

Figure 1 illustrates the test problem. The lens (not shown) is modelled as a singular isothermal ellipsoid with one–dimensional velocity dispersion 260 km s^{-1} and ellipticity $e =$

$1 - b/a = 0.25$. The semi-major axis of the lens is aligned at 40° counterclockwise from the vertical. The Einstein angle is $\theta_E = 4\pi\sigma^2 D_{ds}/(c^2 D_s) = 1.58''$. The source, shown in the top left panel, is contained within a square of size $0.75''$ and is modelled as two circular sources of Gaussian profile, binned in $0.05''$ pixels, the same as the image pixel size. The peak surface brightness of each source is 1.0, in arbitrary units. One source lies inside the inner caustic, while the second source straddles the inner caustic. This source configuration resembles that inferred for the gravitational lens 0047–2808 (Wayth et al., 2003). To create a realistic ACS simulation the image was formed by ray tracing, then convolved with the point spread function, and noise added (in the manner described in the following paragraph). For simplicity we modelled the psf as a Gaussian, and chose FWHM $0.08''$ which is the resolution of a diffraction-limited telescope of the same diameter as HST, at a wavelength $\lambda = 800\text{nm}$. Because of the slight undersampling, the convolution is made on a sub-pixelized grid and then binned up to the full pixel size.

The data pixels used for the inversion were the 3626 pixels within the annulus in the image plane marked in the figure. This annulus is defined by the region covered by imaging the entire source plane.¹ An important point to note is that the analysis region must at least cover this annulus, otherwise the counts in some source pixels will be unconstrained and the inversion will fail. A larger region may be used, but if it becomes too large the usefulness of the χ^2 statistic is diminished, as then most of the pixels are in the background. The final step in the simulation is to apply uniform Gaussian random noise over the image plane. The noise level is defined in terms of the total S/N_{im} integrated over the annulus. The same noise realisation was used for all the simulations, but scaled in order to vary S/N_{im} .

The upper middle panel shows the final simulated ACS image. This image, with source pixel size $0.05''$, $S/N_{im} = 60$, and psf FWHM = $0.08''$, is the reference test problem to invert. We later vary these three parameters. The parameters of the different models we have run are listed in Table 1. Col. (1) provides the simulation number. The reference problem is numbered 1. Col. (2) gives the source pixel size in arcsec, col. (3) the summed S/N in the image, and col. (4) the psf FWHM in arcsec. Col. (5) is a label U or R depending on whether the inversion was unregularized or regularized. Then, in the case of regularized inversion, col. (6) provides the degree of regularization, quantified by the parameter N_λ , which is the increase of $\chi^2_{im}(\nu)$ from the minimum in units of the standard deviation $\sigma(\chi^2_{im}(\nu))$. Recalling the discussion in §1, a value $N_\lambda = 1$ in this column corresponds to the usual criterion for the maximum allowed degree of regularization. The other columns are explained in the next section.

¹The region of the central image should also be included for non-singular mass models.

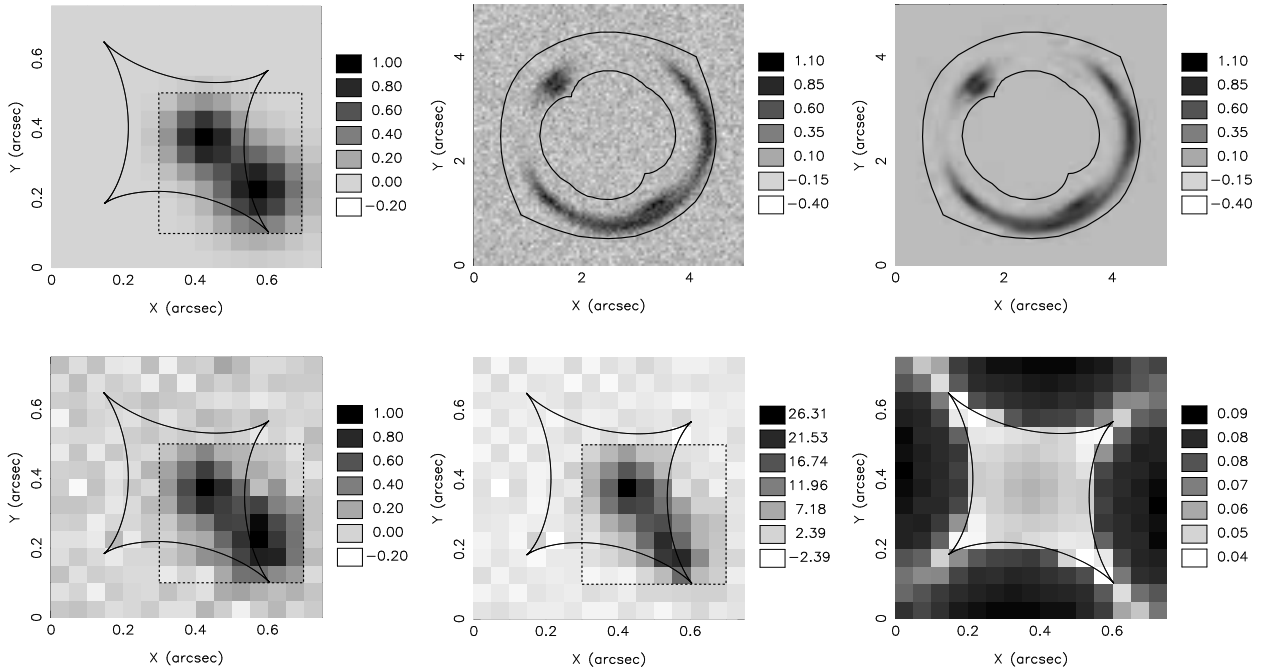


Fig. 1.— This plot shows the unregularized solution for the reference problem, line (1), Table 1. The source plane, top left panel and bottom row, is $0.75'' \times 0.75''$ with $0.05''$ pixels, and is centered on the optic axis. The source comprises two circular Gaussian components and is shown top left. Also marked is the line of the inner caustic for the isothermal ellipsoid lens. The image, convolved with the psf, FWHM $0.08''$, and with noise added, is shown upper middle. The image pixel size is $0.05''$ and the image box size is $5.0'' \times 5.0''$. The lower left panel is the source light distribution reconstructed from the image by semi-linear inversion without regularization. The upper right panel is the image of this source, convolved with the psf. The lower right panel displays the 1σ uncertainty for the source pixels, and the lower middle panel is the source S/N image. The dotted square is the region over which S/N_{so} is measured. In this and the following two figures counts in pixels in both the image and source plane are in units of surface brightness.

(1) sim. no.	(2) source pix. size "	(3) S/N_{im}	(4) psf FWHM "	(5) U/R	(6) N_λ	(7) $\chi^2_{im}(\nu)$	(8) $\chi^2_{so}(\nu)$	(9) S/N_{so}	(10) $ \Delta s/\sigma $ max.	(11) Δs_{rms}	(12) note
1	0.050	60.0	0.08	U		0.956 ± 0.024	1.088 ± 0.094	79.9	2.80	0.082	Fig. 1
2	0.050	30.0	0.08	U		0.956 ± 0.024	1.088 ± 0.094	40.6	2.80	0.163	
3	0.050	60.0	0.00	U		0.958 ± 0.024	1.052 ± 0.094	111.2	2.64	0.040	
4	0.050	60.0	0.16	U		0.956 ± 0.024	1.090 ± 0.094	24.6	2.73	0.252	
5	0.025	60.0	0.08	U		0.952 ± 0.027	1.003 ± 0.047	20.2	2.84	0.634	Fig. 2
6	0.050	60.0	0.08	R	1	0.980 ± 0.024	1.138 ± 0.094	111.8	3.02	0.031	
7	0.050	60.0	0.08	R	2	1.004 ± 0.024	1.461 ± 0.094	120.8	4.35	0.028	
8	0.025	60.0	0.08	R	1	0.979 ± 0.027	1.003 ± 0.047	64.5	3.14	0.242	Fig. 3
9	0.025	60.0	0.08	R	3	1.033 ± 0.027	1.003 ± 0.047	86.6	3.40	0.123	Fig. 3
10	0.025	60.0	0.08	R	5	1.088 ± 0.027	1.004 ± 0.047	98.2	3.34	0.070	

Table 1: Dependence of reconstruction performance on source plane pixel size, simulated ring image noise, psf width, and degree of regularization.

3.2. Fixed mass

The main purpose of the simulations is to illustrate the linear inversion step, the ‘inner cycle’, i.e. that part of the semi-linear inversion method that differs from previous methods. For this reason in this sub-section we fix the mass parameters at the input values. The image inversion, therefore, is achieved in a single step using equations (5) and (12), for the unregularized and regularized cases respectively, and using equations (9) and (17) for the source covariance matrix. We consider the full problem, solving also for the mass parameters in §3.3.

3.2.1. Unregularized inversion

The unregularized inversion of the reference problem is provided in the remaining panels of Figure 1. The lower left panel shows the reconstructed source and the upper right panel shows the image of the reconstructed source convolved with the psf, i.e. the min. $-\chi_{im}^2$ model fit to the simulated image. The bottom right panel shows the source σ image i.e. the standard deviation in each pixel. This provides a visual impression of the uncertainties – note how the region of lowest σ is bounded by the inner caustic. However the whole covariance matrix is required for a proper interpretation of the results. The lower middle panel is the source S/N image. In all the Figures 1 – 3, for the source σ and S/N images the grayscale covers the full range of numbers in the panel. For the other panels the same grayscale range is used in each figure, to allow comparison of the relative noise levels.

We measure several quantities to assess the quality of the inversion, listed in the remaining columns of Table 1. The reduced χ^2 in the image plane, $\chi_{im}^2(\nu)$ is provided in col. (7). The quoted uncertainty is given by $\sqrt{2/\nu}$ where ν is the number of degrees of freedom i.e. the number of image pixels (3626) minus the number of source pixels (225 or 900). The reduced χ^2 in the source plane, $\chi_{so}^2(\nu)$, and its uncertainty, is provided in col. (8). To account for the covariance terms this is computed using

$$\chi_{so}^2 = \sum_{i,k} \Delta s_i \mathbf{C}_{ik}^{-1} \Delta s_k = \sum_{i,k} \Delta s_i \mathbf{F}_{ik} \Delta s_k \quad (18)$$

where Δs_i is the residual in the i th pixel. Here the number of degrees of freedom is the number of source pixels. Col. (9) provides the S/N summed over the small box in the source plane shown in Figure 1. The noise is computed as the square root of the sum of the elements in the covariance matrix, formed by stripping out from the source covariance matrix \mathbf{C} the rows and columns corresponding to the pixels in the box. Col. (10) provides the absolute value of the significance $\Delta s/\sigma$ of the worst-fit source pixel, and col. (11) lists

the *r.m.s.* of the residuals in the source plane.

The results for the reference problem, line (1) in Table 1, are all satisfactory: The reduced χ^2 values in the image and source planes are both consistent with 1.0, and the significance of the worst pixel 2.80σ (col. 10) is not unexpected given that there are 225 source pixels. The summed S/N in the source box is an improvement on S/N_{im} . This might be expected since the box is restricted to the small region of the source plane containing nearly all the signal. At the same time it shows that the S/N is not greatly degraded by amplification of noise in the deconvolution step. We return to this issue below. We interpret these results as meaning that the inversion has succeeded and produced the correct solution to the well-posed problem of finding the source-pixel counts that give the best fit to the image.

In simulation 2 we doubled the noise in the image plane. Comparing lines (1) and (2) in the table, the effect of this is to double the noise in the source plane (col. 11), and so halve the S/N of the detected source (col. 9), as expected.

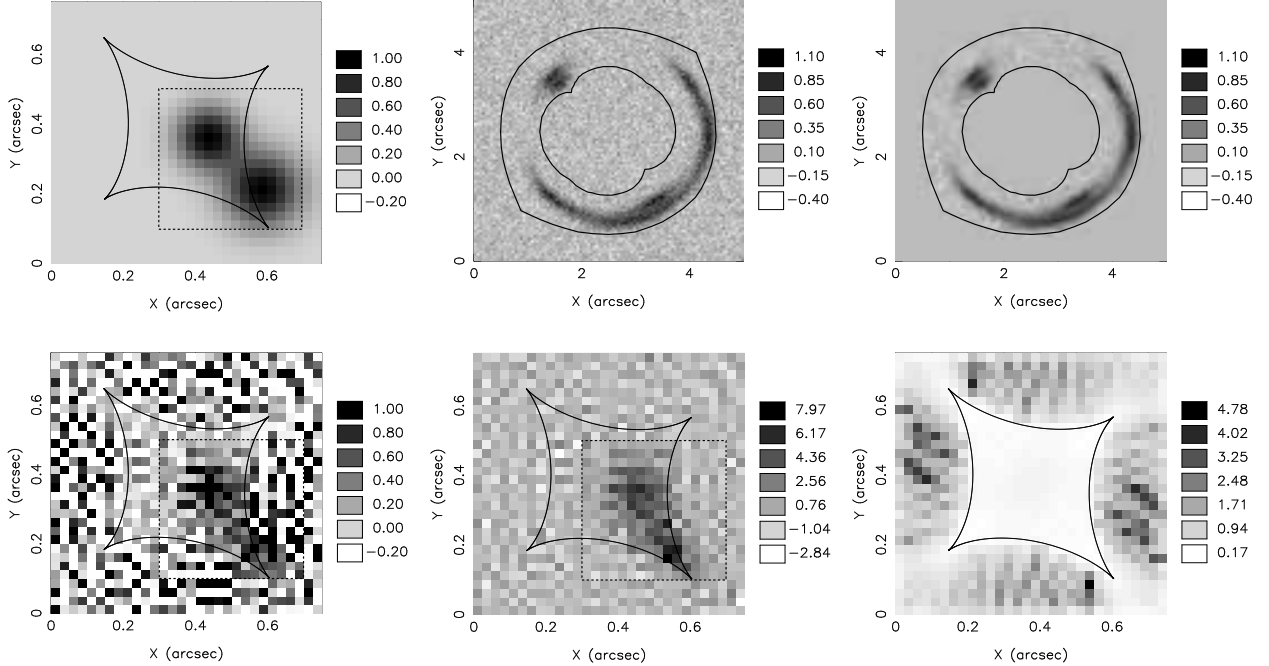


Fig. 2.— The plot shows the unregularized solution for the same problem as in Figure 1, but with source pixels half as large, and corresponds to line (5), Table 1. The source plane, top left panel and bottom row, is $0.75'' \times 0.75''$ with $0.025''$ pixels, and is centered on the optic axis. The source comprises two circular Gaussian components and is shown top left. Also marked is the line of the inner caustic for the isothermal ellipsoid lens. The image, convolved with the psf, FWHM $0.08''$, and with noise added, is shown upper middle. The image pixel size is $0.05''$ and the image box size is $5.0'' \times 5.0''$. The lower left panel is the source light distribution reconstructed from the image by semi-linear inversion without regularization. The grayscale range is the same as in Figure 1. The reconstruction is poor, because the source pixel size is too small. The upper right panel is the image of this source, convolved with the psf. The lower right panel displays the 1σ uncertainty for the source pixels, and the lower middle panel is the source S/N image. The dotted square is the region over which S/N_{so} is measured. In each of Figures 1–3, counts in pixels in both the image and source plane are in units of surface brightness.

Variation of psf FWHM. We have investigated the effect of varying the width of the psf. Line (3) provides the results for no psf, and line (4) provides the results for a psf FWHM of $0.16''$, double the reference value. Comparison of lines (1), (3), and (4) shows that as the psf FWHM increases the noise in the source plane, col. (11), increases and the source detection S/N , col. (9), decreases. This is as expected: In Fourier space the effect of the psf is to suppress the amplitude of the power spectrum of the source for large wave numbers. Therefore in the deconvolution process the noise on these scales is amplified. As the psf is broadened the power suppression is greater, and so the noise amplification in the deconvolution step is greater. The reduction in S/N_{so} from 111.2 (line 3) to 79.9 (line 1), in going from no psf to psf FWHM of $0.08''$, is quite modest. This demonstrates that satisfactory inversion of ACS images using $0.05''$ source pixels is possible without regularization.

Regardless of the degree of amplification of noise the various statistical quantities in cols (7)–(11) of Table 1, lines (1)–(4), are all reasonable. This shows that in these cases the inversion is well behaved, and in none of the cases is the matrix \mathbf{F} singular. This contrasts with the usual inversion problem, for example image deconvolution. With image deconvolution the number of parameters to solve for (the counts in the deconvolved image pixels) is typically the same as or greater than the number of constraints (the number of image pixels). In lensing, because of magnification, the number of image pixels may be much greater than the number of source pixels. This suggests, further, that in regions where the magnification is greatest it would be possible to use source pixels smaller than the image pixels. We consider this issue below.

The results of these first four simulations indicate that, in some circumstances, provided the psf is not too broad, unregularized semi-linear inversion provides a useful solution.

Variation of source pixel size. Figure 2 shows the same problem as Figure 1 but with $0.025''$ source pixels rather than $0.05''$ pixels. The results are summarized in line (5) of Table 1. The quality of the reconstruction, lower left panel, is now dramatically worse, and outside the central region is clearly unsatisfactory. (The grayscale range of this panel is the same as in Figure 1.) Compared to line (1) the noise in the source (col. 11) has risen by a factor 8, whereas intuitively one would expect only a factor 2 increase (4 times as many pixels). This is indicative of large amplification of noise, because the psf has suppressed the signal on these scales. This is a consequence of the fact that the separation in the image plane of the images of two adjacent source pixels is smaller than the psf size. Put another way, a resolution element in the image plane, traced back to the source plane, is oversampled by the source pixel size. The source covariance matrix now contains large, predominantly negative, covariance terms which correspond to the odd/even appearance in the outer regions of the source plane.

The high noise level in the outer parts of the source–plane belies the usefulness of this image. In fact the source is strongly detected, albeit at reduced $S/N_{so} = 20$, even though not readily apparent to the eye. The source is clearly visible in the S/N image, however. At the same time the χ^2 values in both the image and source planes remain satisfactory. Because of the larger magnification, the reconstruction is much better within the caustic line. This suggests it would be advantageous to use a variable pixel size across the source plane. For example, with reference to Figure 2, a scheme where the pixel size is $0.05''$ outside the caustic and $0.025''$ inside might be appropriate. We need to identify a criterion for choosing the pixel size that avoids the excessive amplification of noise evident in Figure 2. There are clearly three variables which determine the minimum source pixel size: The image pixel size, a , the psf FWHM, b , and the magnification, c . We have had some success with a scheme which relates the source pixel size to the variable $\max(a, b/2)/c^{1/2}$. The results will be reported elsewhere (Dye and Warren, in prep.).

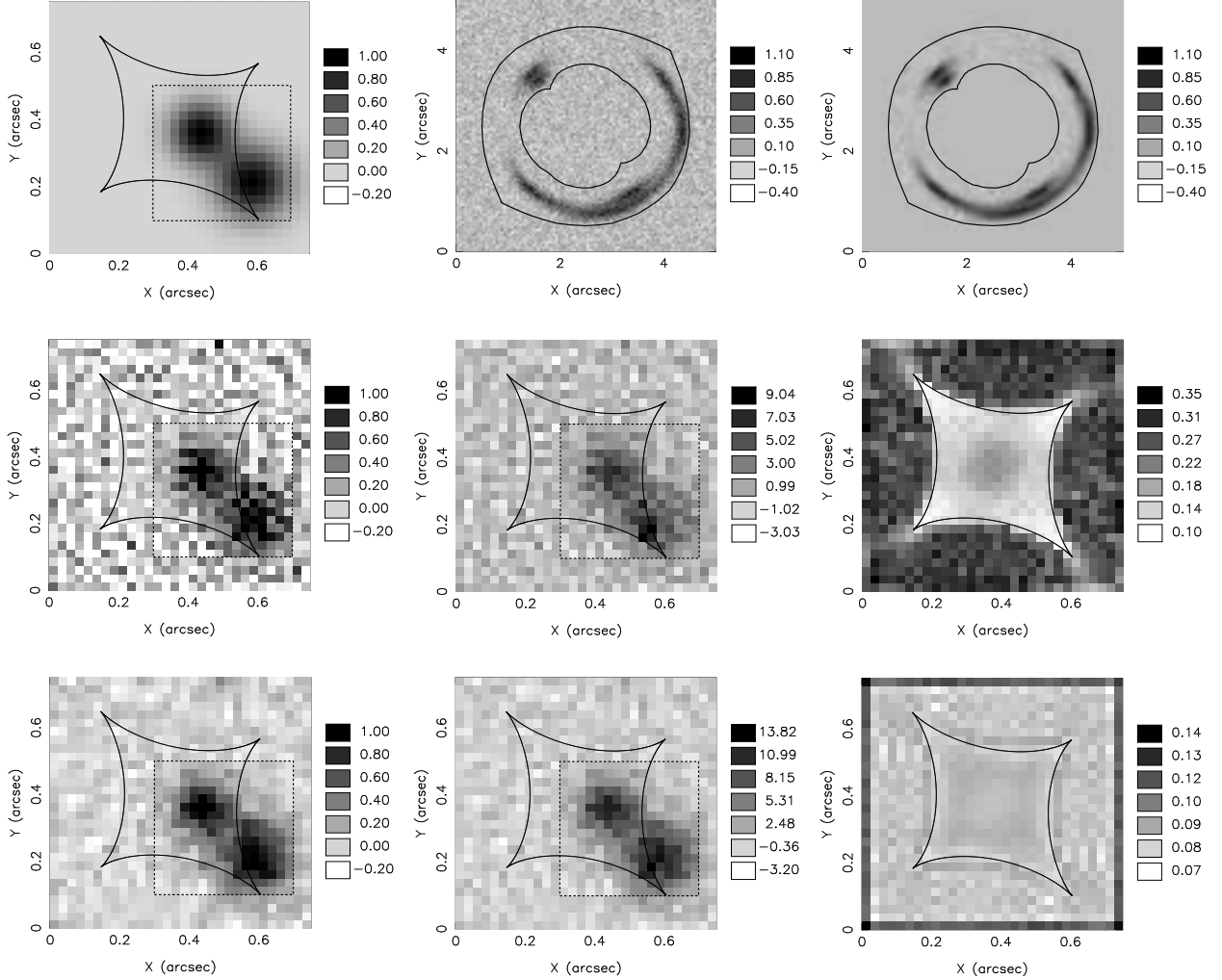


Fig. 3.— The plot shows regularized solutions for the same problem as in Figure 2, with different degrees of regularization. The middle row is for $N_\lambda = 1$ (corresponding to line (8) of Table 1), and the bottom is for $N_\lambda = 3$ (line (9) of Table 1). The source plane, top left panel, and middle and bottom rows, is $0.75'' \times 0.75''$ with $0.025''$ pixels, and is centered on the optic axis. The source comprises two circular Gaussian components and is shown top left. Also marked is the line of the inner caustic for the isothermal ellipsoid lens. The image, convolved with the psf, FWHM $0.08''$, and with noise added, is shown upper middle. The image pixel size is $0.05''$ and the image box size is $5.0'' \times 5.0''$. The left middle panel is the source light distribution reconstructed from the image by semi-linear inversion with regularization, $N_\lambda = 1$. The solution is much less noisy than the unregularized solution, Figure 2. The upper right panel is the image of this source, convolved with the psf. The middle right panel displays the 1σ uncertainty for the source pixels. The center panel of the middle row is the source S/N image. The bottom row is the set of corresponding source-plane images for the case $N_\lambda = 3$. Note the larger errors in the outermost band in the bottom right panel. This is a consequence of the choice of a gradient regularization term, since these pixels have fewer neighbours. The dotted square is the region over which S/N_{so} is measured. In each of Figures 1–3, counts in pixels in both the image and source plane are in units of surface brightness.

3.2.2. Regularized inversion

We now include linear regularization in the inversion. All the results reported here used the gradient form, equation (14). The results are quite similar for the different linear regularizing schemes described in §2.1.1, however.

Lines (6) and (7) in Table 1 are the results for the reference problem with different degrees of regularization. As the regularizing term increases, the source becomes smoother and χ_{im}^2 increases. Line (6) is for $N_\lambda = 1$. Comparing line (6) to line (1) we see that the effect of regularization is to suppress the noise in the reconstructed source and to increase substantially the source S/N , col. (9). This is at the expense of a poorer match to the true source light profile, as measured by cols (8) and (10). For $N_\lambda = 2$ the agreement with the input source is no longer acceptable.

In lines (8) to (10) we provide solutions for source pixel size $0.025''$, and psf FWHM of $0.08''$, and different degrees of regularization, $N_\lambda = 1, 3, 5$. These results compare directly to the unregularized solution to the same problem, line (5). The solutions for simulation no. 8, $N_\lambda = 1$, and no. 9, $N_\lambda = 3$, are shown in Figure 3. The visual improvement, comparing the sequence of Figure 2 (unregularized), Figure 3 middle row (regularized, $N_\lambda = 1$), and Figure 3 bottom row (regularized, $N_\lambda = 3$), is dramatic.

Comparing lines (8) to (10) against line (5) we see that, again, regularization successfully suppresses noise, increasing the S/N of the detection of the source. As N_λ increases, in this case χ_{so}^2 increases only very slowly, much more slowly than in the case for larger pixels. This is partly due to the fact that we chose a smooth source, and the results would be different for a source with more small-scale structure. Nevertheless, it indicates that the standard criterion for the degree of regularization to apply, $N_\lambda = 1$, is somewhat arbitrary.

To summarise this sub-section, using a realistic problem, we have validated the theory of the linear inversion step set out in §2. This is the step that differs from the maximum-entropy method of Wallington et al. (1996), and therefore is the main point of the paper.

3.3. Mass cycle

In the present sub-section we report the results of solving the complete problem i.e. determining both the mass profile and the source light distribution.

We first consider the unregularized case. Referring back to the example of Figure 1, the problem is to invert the image at upper middle. The free parameters are the five parameters describing the mass: x , y , ellipticity, position angle, and velocity dispersion. We searched

through the parameter space to find the min.– χ^2 fit. At the minimum the matrix \mathbf{F} supplies most of the terms of the curvature matrix. Following the precepts of §2.1.2, the remaining terms were filled in by measuring the relevant second partial derivatives of the χ^2 surface. We found the surface to be completely smooth and parabolic near the minimum. The full curvature matrix was inverted to obtain the full covariance matrix for all the parameters, the mass terms as well as the counts in the source pixels. We found the input mass parameters were correctly recovered to within the uncertainties. We checked the full covariance matrix against the results of Monte–Carlo simulations and found excellent agreement. This confirms that, provided the chosen source pixel size is not too small, the unregularized semi–linear inversion method is a practical solution to the problem of inversion of a gravitational lens image with a resolved source.

We also compared the terms in the *source covariance matrix* $\mathbf{C} = \mathbf{F}^{-1}$ against the corresponding terms in the *full covariance matrix*. The differences are relatively small. Therefore the matrix \mathbf{C} , at the global minimum, provides an approximation to the true source–pixel errors that may be very useful in the exploration stage, when considering different mass models and different pixelizations.

In the regularized case we found, generally, that the procedure converged more rapidly than in the unregularized case. Regularized inversion can produce solutions which are not true representations of the source (§3.4, Table 1). Nevertheless, we found, in contrast, that the solution for the mass parameters is very insensitive to the degree of regularization. In the regularized case, the curvature of the merit function cannot be used to obtain the full covariance matrix so that an alternative approach such as a Monte Carlo method must be adopted (§2.2.2). So the source covariance matrix, equation (17), at the global minimum, is particularly useful here as an approximation to the true source–pixel errors.

3.4. Regularized *vs* unregularized

We now include a debate on the relative advantages of the unregularized and regularized approaches. This may seem surprising given the excellent results achieved with regularization (comparing Figures 2 and 3). The weakness of the unregularized inversion is that in deconvolving the psf, the noise at large wavenumbers is boosted. The regularization term in the merit function imposes smoothness on the solution. In effect, the deconvolution (division in Fourier space) is limited to the smaller wave numbers. However, this means that any real structure in the source at large wavenumbers is also suppressed. We are imposing a prejudice that the source is smooth and this might not be justified (see comments in §1). Regularization introduces +ve covariance between adjacent pixels, forcing the counts to be

similar. The regularized solution, then, is not so different to the unregularized solution with larger pixels. In this respect, it is interesting to compare the unregularized solution with $0.05''$ source pixels (Figure 1), with the $N_\lambda = 1$ regularized solution with $0.025''$ source pixels (Figure 3). Noting that the two values of the source S/N are quite similar (79.9, 64.5, respectively, Table 1), it is a debatable point whether there is more information in the latter figure.

A further point to note is that the regularized inversion can produce solutions which are satisfactory in terms of the fit to the image but which are not true representations of the source in the sense that the χ^2_{so} is unsatisfactory. For example in line (7), Table 1, both χ^2_{so} and $|\Delta s/\sigma|$ are unsatisfactory. Measured by the same statistics, none of the unregularized inversions in the Table is unsatisfactory. The unregularized inversion gives a noisier but unbiased solution for the source light distribution, while the regularized inversion gives a smoother but biased solution.

Despite regularization biasing the source, in the full mass cycle we find that the minimized mass parameters show little sensitivity to the degree of regularization. Furthermore, the regularized solution has the advantage that it converges more quickly. We discuss the practical significance of these two points in §4. Associated with this is the fact that regularization allows source pixel sizes of almost any size, unlike the unregularized case when pixel size must be chosen carefully. This can yield further speed advantages in the initial stages of an analysis, before the solution is refined.

Overall we consider there are important advantages to using both regularized and unregularized inversion in exploring the solution to a particular problem, and the choice will depend on the question being posed and any a priori knowledge concerning the source. Perhaps equally importantly, however, it makes sense to match the source pixel size to the data information content in terms of the S/N at different wavenumbers, or, in other words, to vary the pixel size depending on the magnification, as suggested in §3.2.1.

4. Summary and recommendations

We have developed a new method for the inversion of gravitationally-lensed images of extended sources for the case where the source light profile is pixelized. The method separates the linear dimensions of the problem (the counts in the source pixels) from the non-linear dimensions (the mass parameters). The method has been extended in a natural way to allow linear regularization of the inversion. The core of the routine is the procedure for inverting an image given a fixed mass profile. We have shown that this step, including

deconvolution of the psf, with or without regularization, is a linear one. Since this step is usually achieved by searching the source parameter space for the merit–function minimum, the solution is reached much more quickly. The non–linear part of the problem has been reduced to the search for a minimum in the space of the mass parameters only. In the case of unregularized inversion, the full covariance matrix for all the (source+mass) parameters can be obtained very quickly. In the case of regularized inversion, a useful approximation to the covariance matrix for the source counts is obtained very simply, but Monte Carlo methods are needed to obtain the full covariance matrix.

How the semi–linear method should be applied in practice depends on the problem posed. If one is interested in the quantitative details of the source light profile, for example, whether some apparent feature is real, then we recommend the unregularized solution. This is because regularization produces source profiles which are too smooth. Without regularization, an optimal source pixel size should be chosen. Having too large a source pixel may cause interesting detail to be lost. However, if the source pixel size is too small, the inverted image may have low S/N because of amplification of noise in the deconvolution step. If, on the other hand, one is interested only in the mass parameters, a regularized solution would be the appropriate choice: The mass parameters are rather insensitive to the degree of regularization and one benefits from an increase in inversion speed.

Another consideration is that pixelizing the source uses a large number of parameters. As a rule, one is interested in finding the model with the smallest number of parameters that provides a satisfactory fit to an image. Therefore, in many cases, one might simply use the semi–linear method of inversion to provide an image of the source to guide the choice of parameterization. Here, again, the regularized solution might be the preferred option.

In general, because it is so much easier to implement (§2.2.1), we recommend using zeroth–order regularization. Nevertheless, other considerations may override simplicity. The zeroth–order regularization term, in common with the maximum–entropy regularization term, is a local measure, independent of the counts in adjacent pixels. This can be an advantage or a disadvantage, depending on the actual light profile in the source.

In the simulations presented here, we have used square source pixels which form a regular grid. However, since the resolution across the image plane is fixed while the magnification varies, the resolution across the source varies. Therefore, to maximize the information content in the reconstruction of the source it is necessary to use a variable source pixel size. We will present an analysis of semi–linear inversion with variable source pixel size in a future paper (Dye and Warren, in prep.).

We have benefited from discussions with Paul Hewett, Geraint Lewis, Leon Lucy, and

Randall Wayth.

REFERENCES

Kayser, R. & Schramm, T., 1988, A&A, 191, 39

Kochanek, C.S., Blandford R.D., Lawrence C.R., & Narayan, R., 1989, MNRAS, 238, 43

Press, W.H., Teukolsky, S.A., Vetterling, W.T., & Flannery, B.P., 2001, 'Numerical Recipes in Fortran 77, 2nd Edition', Cambridge University Press

Tyson, J.A., Kochanski, G.P., & dell'Antonio, I.P., 1998, ApJ, 498, 107

Wallington, S., Kochanek, C.S., & Koo, D., 1995, ApJ, 441, 58

Wallington, S., Kochanek, C.S., & Narayan, R., 1996, ApJ, 465, 64

Wayth, R.S., Warren, S. J., Lewis, G.F., & Hewett, P.C., 2003, MNRAS, in preparation